Hindawi
Journal of Nanomaterials
Volume 2017, Article ID 6839474, 11 pages
https://doi.org/10.1155/2017/6839474

Research Article

Fabrication of Amino Functionalized Magnetic Expanded Graphite Nanohybrids for Application in Removal of Ag(I) from Aqueous Solution

Ying-Xia Ma, Yong-Xin Ruan, Dan Xing, Xue-Yan Du, and Pei-Qing La

State Key Laboratory of Advanced Processing and Recycling of Non-Ferrous Metals, Key Laboratory of Nonferrous Metal Alloys and Processing, Ministry of Education, School of Materials Science & Engineering, Lanzhou University of Technology, Lanzhou 730050, China

Correspondence should be addressed to Ying-Xia Ma; mayx2011818@163.com and Xue-Yan Du; duxy@lut.cn

Received 19 September 2016; Revised 21 December 2016; Accepted 25 December 2016; Published 9 February 2017

Academic Editor: Xuping Sun

Ethylenediamine functionalized magnetic expanded graphite decorated with Fe_3O_4 nanoparticles (MEG-NH_2) was fabricated by one-pot solvothermal method. The as-prepared MEG-NH_2 nanohybrids were characterized by means of scanning electron microscopy (SEM), X-ray diffraction (XRD), Fourier transform infrared spectra (FTIR), X-ray photoelectron spectroscopy (XPS), thermogravimetric analysis (TGA), vibrating sample magnetometer (VSM), and Zeta potential analyzer. The effects of Fe_3O_4 content in MEG-NH_2 nanohybrids, pH, initial concentration, contact time, and dosage on adsorption properties of the MEG-NH_2 nanohybrids for Ag(I) from aqueous solution were investigated by batch experiments. The pseudo-first-order and the pseudo-second-order kinetic models were utilized to study adsorption kinetics. The experimental data was also analyzed with Langmuir, Freundlich, Temkin, and Dubinin–Radushkevich isotherm models. The results show that Ag(I) was reduced to silver in the process of the adsorption by MEG-NH_2 nanohybrids; the experimental data was better fitted to pseudo-second-order model and Langmuir isotherm model which revealed that the adsorption process was a chemical adsorption by the formation of silver on the surface of MEG-NH_2 nanohybrids.

1. Introduction

In recent years, numerous water bodies such as rivers, lakes, and ponds have accommodated a great deal of waste water composed of industrial and domestic sewage. Among various contaminants, heavy metal ions occupy a large proportion. Drainage of high concentration of heavy metal ions is extremely deleterious to living organism and the environment, especially to the existence and development of human beings, which has aroused global concerns. Among heavy metals, sliver is not dietary requirement for organic survival. Englobement of high level of silver is toxic to human cells. Ag(I) is more fatal for fish than copper or mercury [1]. On the other hand, as a precious metal, silver possesses extensive commercial value in various fields for its unique ornament and decoration performance and highest electrical and thermal conductivity along with excellent machinability [2]. Given the above notable properties, the widely technical and industrial usage of silver in photography, brazing, electronic products, electroplation, and so forth heavily accelerates its requirements. However, with surging demand of silver, silver bearing mines that are available for exploitation have reached a steep reduction. Moreover, substantial employment of silver in various industries inevitably creates mass production of silver-containing effluent. To dispose the thorny issue, a large number of measures have been taken, including adsorption, cathodic reduction [3], ion-exchange [4], solvent extraction [5], and so on. During the past decade, adsorption method has attracted much attention in heavy metal removal and recycling [6] for its energy saving, high efficiency, and outstanding selectivity, especially its superiority in disposal of trace metal ions. Currently, various adsorbents have been utilized to treat waste water containing silver ions, such as chitosan [7], ion-imprinted polymers [8], zeolite, chemically

modified melamine resins [9], and bioadsorbent [10]. It is somewhat difficult for these traditional adsorbents to separate for resource recycling after adsorption. The magnetic adsorption materials solve the practical problem.

Magnetic expanded graphite (MEG) holds lower price and easier preparation properties compared with graphene, carbon nanotubes, and other carbonaceous adsorbents, arousing researchers' extensive interests [11, 12]. Generally, the synthesis process of MEG with a majority of macropores and favorable magnetic response is composed of oxide intercalation, high temperature expansion, and magnetic loading. The resulting macropores formed in the interlayers, providing passageway for ion diffusion. Acquisition of magnetic performance avoids centrifugation, decompressed filter, and slather usage of expensive percolators. With a weak magnet, it is very simple and effective to separate the material along with target contaminant. Thus, secondary pollution will never occur, and the recovery and recycling of silver are ready to be realized [13]. Nevertheless, it is not ideal for pure MEG to be applied to adsorb silver ions owing to lack of appropriate functional groups. These materials mostly need modification to improve their physicochemical properties. Accordingly, it is necessary to graft suitable functional groups onto surface of MEG to introduce active sites for silver ion adsorption.

In this study, using ethylenediamine functionalized magnetic expanded graphite (MEG-NH_2) nanohybrids with desirable performance composed of magnetism of Fe_3O_4, chemical adsorption of amino groups, and unique ion diffusion channels of EG were synthesized by one-pot solvothermal reaction. In contrast to chemical coprecipitation method [14], the approach prevented oxidation and aggregation of nano-Fe_3O_4. The effects of Fe_3O_4 content in MEG-NH_2 nanohybrids, pH, initial concentration, contact time, and dosage on the adsorption properties of the MEG-NH_2 nanohybrids for Ag(I) were taken into consideration during adsorption experiments. Adsorption kinetics and isotherms were also studied to ascertain the adsorption process.

2. Experimental

2.1. Materials and Chemicals. Natural flake graphite (NFG), 50 BS mesh, with the purity of 99 wt% was supplied by ShanDong Qingdao Tianhe Graphite Company (China). Concentrated sulfuric acid (H_2SO_4), concentrated nitric acid (HNO_3), potassium permanganate ($KMnO_4$), ferric chloride hexahydrate ($FeCl_3{\cdot}6H_2O$), sodium acetate anhydrous, ethanediol, ethylenediamine, ethanol, potassium hydroxide, potassium periodate, and potassium sulfate are all of analytical grades, used as received without any further purification.

2.2. Preparation of Expanded Graphite. Expanded graphite (EG) was prepared according to our previous work [15]. NFG (20 g) was added to the mixture mingled with 70% H_2SO_4 (45 g) and 68% HNO_3 (15 g) in a 250 mL three-neck flask. Subsequently, $KMnO_4$ (2.2 g) was put into the mixture within several times under vigorous stirring. After reaction for 50 min, the products were collected with high-speed centrifuge and washed with deionized water till the filtrate turned into neutrality. Then, the as-prepared product was dried in vacuum at 50°C for 24 h. Finally, the above dried sample was heat treated abruptly at 600°C for 15 s to obtain EG.

2.3. Preparation of MEG-NH_2 Nanohybrids. MEG-NH_2 nanohybrids were synthesized by using one-pot solvothermal method as follows. Firstly, different contents of $FeCl_3{\cdot}6H_2O$ (0.8 g, 1.0 g, and 1.2 g) and sodium acetate (3.0 g) were fully dissolved into a 100 mL beaker containing ethanediol (20 mL), and then ethylenediamine (10 mL) was added under stirring. The mixture turned into transparent yellowish color after ultrasonic oscillation was exerted. The above solution was transferred into a Teflon lined stainless steel autoclave containing EG (0.15 g) with vigorous agitation. The container was sealed and heated to 200°C for 8 h in a muffle furnace and then cooled to room temperature. The black product was washed several times with ethanol by applying an external magnetic field. Ultimately, the obtained different contents of Fe_3O_4 of MEG-NH_2 nanohybrids were dried in vacuum at 50°C for 24 h. Fe_3O_4-NH_2 was prepared by the process mentioned above in the absence of EG.

2.4. Characterization. The scanning electron microscopy (SEM) images taken with a JEOL JSM-6701 field emission scanning electron microscope (FESEM, 5 kV) were applied to observe the external morphology of samples. X-ray diffraction patterns (XRD, Rigaku D/MAX-2400 X-ray diffractometer with Ni-filtered Cu Kα radiation (λ = 1.54056 Å)) were performed to detect the crystal structure of samples. Fourier transform infrared spectroscopy spectra (FTIR) were recorded on a NEXUS 670 spectrometer with samples pressed into KBr pellets. X-ray photoelectron spectroscopy (XPS) analysis was carried out to detect the adsorbents before and after adsorption. Thermogravimetry analyzer (TGA, STA449C, Netzsch, Germany) was performed to investigate the thermal stability of samples. Hysteresis loops were obtained by a vibrating sample magnetometer (VSM) which was employed to perform magnetic properties of as-synthesized samples. Zeta potential was measured in a Malvern Zetasizer by dispersing the sorbent in deionized water with different pH values. Ultraviolet spectrophotometer (UV-752N) was used to measure the absorbance of Ag(I) at 365 nm.

2.5. Adsorption Experiments. Adsorption experiments were carried out with a typical batch approach. $AgNO_3$ was used as source of Ag(I). Various parameters including pH, contact time, dosage, and temperature were investigated. The pH was adjusted to certain values by dropping different concentrations of HNO_3 and NaOH aqueous solution. The concrete procedure was according to the following method: a certain amount of adsorbent was added to a 250 mL conical flask containing $AgNO_3$ aqueous solution of 50 mL at a known concentration accompanied with manual shaking rather than ultrasonic dispersion to keep the original morphology of samples. After that, the aforementioned conical flask sealed with preservative film was fastened to a platform constant rate of 120 rpm in a thermostat oscillator under dark environment.

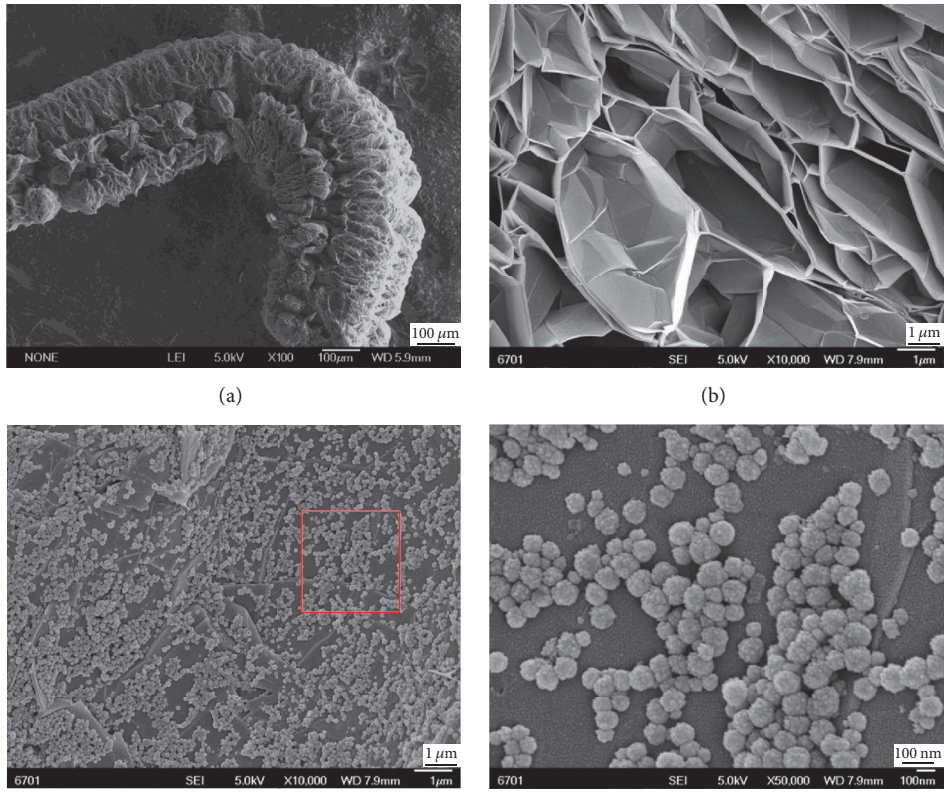

Figure 1: SEM images of EG (a, b) and MEG-NH_2 nanohybrids (c, d) under different magnification.

Magnet was employed to pull the adsorbent down to acquire supernatant to test absorbance with an ultraviolet-visible spectrophotometer when the platform constant shaking incubator was reached at the given time.

In order to reduce detection errors, absorbance of each sample was under triplicate measurements, the mean value of which was used to calculate adsorption capacity of adsorbent and removal efficiency according to the following equations [16, 17]:

$$Q = \frac{(C_0 - C) \times V}{m}$$
$$R = \frac{(C_0 - C) \times 100\%}{C_0}, \quad (1)$$

where Q is adsorption capacity of Ag(I) on MEG-NH_2 nanohybrids ($mg \cdot g^{-1}$), R is removal efficiency, C_0 and C are initial and outlet concentration of Ag(I) in solution ($mg \cdot L^{-1}$), respectively, V is the volume of the added Ag(I) aqueous solution (mL), and m is dosage of the adsorbent (mg).

3. Results and Discussion

3.1. Morphological and Structural Studies of MEG-NH_2 Nanohybrids. SEM analysis was performed on the as-obtained samples to determine the features under micro-nano-scale. Figure 1 shows the SEM images of EG and MEG-NH_2 nanohybrids under different magnification. After oxidation and high temperature expansion, NFG was transformed into worm-like EG, which presents loose and porous structure (Figure 1(a)). A corresponding high-magnification SEM image (Figure 1(b)) of the EG displays a distinct flexible interleaved structure. After solvothermal reaction, the surface of EG was loaded with dimensionally homogeneous Fe_3O_4 nanoparticles, the average diameter of which is close to 100 nm (Figure 1(c)). Interestingly, the monodispersed Fe_3O_4 nanoparticles are composed of many smaller Fe_3O_4 nanoparticles, as shown in Figure 1(d), which is the magnification of circled pattern in Figure 1(c).

XRD was employed to ascertain the phase and structure of the as-synthesized samples. Figure 2 presents XRD patterns of EG (a), MEG-NH_2 nanohybrids (b), and MEG-NH_2 nanohybrids after adsorption of Ag(I) (c). In Figure 2(a), the peak approximate to $2\theta = 26.5^\circ$ is attributed to crystal face (002) of graphite [18, 19]. Besides, (101) and (004) faces appearing at $2\theta = 44.6^\circ$ and 54.9° are also the characteristic diffraction faces of graphite, which is in line with JCPDS card number 41-1487. After one-pot solvothermal reaction, the (220), (311), (400), (422), (511), and (440) planes of Fe_3O_4 are observed at $2\theta = 30.1^\circ$, 35.5°, 43.2°, 53.4°, 57.0°, and 62.6°, respectively [20, 21], according to JCPDS card number 89-4319 for the magnetite (Figure 2(b)). What is more, the diffraction peaks mentioned above are ascribed to inverse spine crystalline structure of Fe_3O_4 [22]. MEG-NH_2

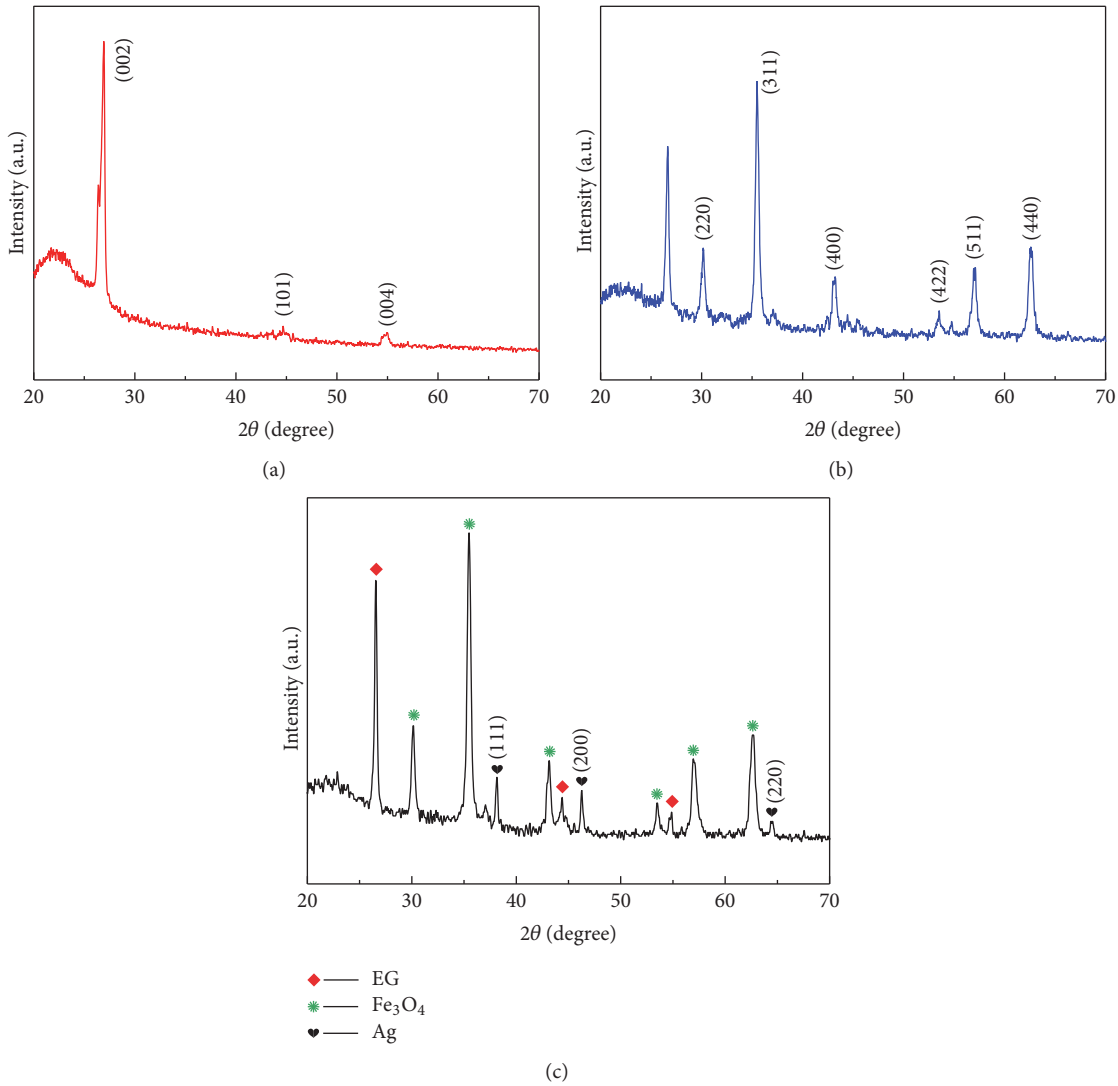

Figure 2: XRD patterns of EG (a), MEG-NH_2 nanohybrids (b), and MEG-NH_2 nanohybrids after adsorption of Ag(I) (c).

nanohybrids after adsorption of Ag(I) and new diffraction planes (111), (200), and (220) of silver are observed at 2θ = 38.2°, 44.4°, and 64.6° (Figure 2(c)) according to JCPDS card number 87-0720. The results reveal that Ag(I) was reduced to elemental silver in the process of the adsorption by MEG-NH_2 nanohybrids.

Figure 3 shows the FTIR spectra of EG and MEG-NH_2 nanohybrids. The spectrum shows that the major FTIR adsorption peaks of EG are at 3434 cm^{-1}, 1630 cm^{-1}, and 1408 cm^{-1}, which are attributed to stretching vibration of the -OH group on the surface of EG, aromatic C=C, and methylene, respectively [18]. The formation of EG is due to high temperature expansion of graphite oxide and so are oxygen-containing functional groups on the surface of EG. The peak at 1110 cm^{-1} is assigned to stretching vibration of C-O-C [23].

However, in comparison with EG, MEG-NH_2 shows totally different FTIR vibrations. The peaks at 2922 cm^{-1} and 2853 cm^{-1} correspond to asymmetric and symmetric stretching of -CH_2 group of ethylenediamine, which provide the presence of ethylenediamine on MEG surface. The appearance of peaks at 1621 cm^{-1} (bending vibration of N-H), 1574 cm^{-1} (deformation vibration of N-H), and 1193 cm^{-1} (stretching vibration of C-N) further indicate that the ethylenediamine was successfully grafted on the surface of MEG nanohybrids.

XPS analysis was initially conducted for adsorbents prior to adsorption in order to characterize the available functional groups and to characterize the functional groups involved in the adsorption mechanisms [24]. XPS spectra of both survey of MEG-NH_2 nanohybrids (before and after Ag(I) adsorption) and high-resolution scans for Ag3d, C1s, and N1s were measured, as shown in Figure 4. From the survey spectra (Figure 4(a)), it can be seen that the chief elements in MEG-NH_2 nanohybrids include C, N, O, and Fe, which is also in agreement with FT-IR spectra. After adsorption, the presence of Ag3d on the spectrum of MEG-NH_2 nanohybrids clearly confirms the successful adsorption of Ag(I). Figure 4(b)

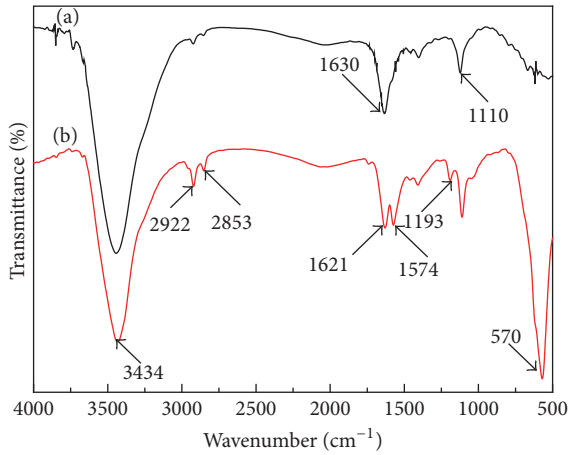

Figure 3: FTIR spectra of EG (a) and MEG-NH_2 nanohybrids (b).

shows Ag3d spectrum, where a pair of doublet-peaks appear, which could be assigned to $Ag3d_{3/2}$ and $Ag3d_{5/2}$ of silver with binding energies at 374.2 eV and 368.2 eV, respectively. This result is in accordance with the XRD analysis that Ag(I) was reduced to elemental silver in the process of the adsorption by MEG-NH_2 nanohybrids.

As shown from Figures 4(c) and 4(d), the C1s spectra do not show any significant changes before and after adsorption. But the N1s spectra changed obviously. Before adsorption, the peaks at 399.9 eV and 400.6 eV are ascribed to -NH_2 and NH_3^+ which is the outcome generated from -NH_2 protonation [25]. After adsorption, the two peaks are transformed to 397.7 eV and 399.8 eV, respectively. Besides, the peak area ratio between -NH_2 and NH_3^+ is changed from 1 : 0.33 to 1 : 2.40. This phenomenon can be attributed to the formation of NH-Ag complexes; in detail a lone pair of electrons in the nitrogen atom is provided to the shared bond between the N atom and Ag. As reported [26, 27], heavy metal ions like Ag^+ with a high standard reduction potential can be reduced to metals by some functional groups like -NH_2, -CN, and so forth.

To investigate the thermal stability of synthesized samples, TGA was performed in nitrogen atmosphere with a heating rate of 10°C·min^{-1}. Figure 5 shows the TGA curves of EG (a), Fe_3O_4-NH_2 (b), MEG-NH_2 nanohybrids prepared with 1.2 g (c), 1.0 g (d), and 0.8 g (e) $FeCl_3{\cdot}6H_2O$. As shown in Figure 5(a), the TGA curve of EG presented three stages: the first stage is due to the loss of adsorbed water and gas molecules from 50°C to 150°C; the second stage is attributed to the decomposition of oxygen-containing functional groups from 150°C to 430°C [28]; the third stage is associated with the removal of more stable oxygen functionalities [15]. The weight loss throughout the process was 12%. The TGA curve of Fe_3O_4-NH_2 (Figure 5(b)) presented two stages: the first stage is due to the removal of adsorbed water below 200°C; the second stage is associated with the degradation of amino functional groups from 200°C to 340°C. The weight loss throughout the process was closed to 12%. For MEG-NH_2 nanohybrids, the mass loss below 135°C was related to the evaporation of absorbed water and gas molecules. With the increasing of temperature, they displayed a gradual mass loss in the range of 135°C to 350°C, which can be referred to the degradation of oxygen-containing functional groups as well as amino functional groups on the surface of nanohybrids. With the temperature increasing sequentially, there was further mass loss due to the bulk pyrolysis of the stable functional groups [29]. The weight loss of MEG-NH_2 nanohybrids increased with the decreasing of $FeCl_3{\cdot}6H_2O$ addition. From Figure 5, we calculate that the Fe_3O_4 contents in MEG-NH_2 nanohybrids prepared with 1.2 g, 1.0 g, and 0.8 g $FeCl_3{\cdot}6H_2O$ were 43.2%, 35.2%, and 32.9%, respectively.

Table 1: Effect of Fe_3O_4 content in MEG-NH_2 nanohybrids on the adsorption of MEG-NH_2 nanohybrids for Ag(I).

Fe_3O_4 content in MEG-NH_2 nanohybrids (%)	Q (mg·g^{-1})
0	16.886
32.9	76.395
35.2	82.692
43.2	73.561
100	13.737

3.2. VSM. The vibrating sample magnetometer (VSM) was applied to test the magnetic property of pure Fe_3O_4 nanoparticles and MEG-NH_2 nanohybrids, as shown in Figure 6. The saturation magnetizations of Fe_3O_4 nanoparticles and MEG-NH_2 nanohybrids are 59.6 emu·g^{-1} (Figure 6(a)) and 34.6 emu·g^{-1} (Figure 6(b)), respectively. Obviously, the presence of EG should be responsible for the decrease of overall magnetic performance. Coercivities of the two samples are approximate to zero, which shows that Fe_3O_4 nanoparticles and MEG-NH_2 nanohybrids have superparamagnetism. Figure 6(c) shows a photograph of MEG-NH_2 nanohybrids dispersed in the water (left) and exerting an external magnetic field (right). In the presence of external magnetic field, MEG-NH_2 nanohybrids are attracted to the wall of the bottle swiftly, which caters separation demand from aqueous solution.

3.3. Adsorption Properties

3.3.1. Effect of Fe_3O_4 Content in MEG-NH_2 Nanohybrids. In order to optimize the preparation condition of MEG-NH_2 nanohybrids, Fe_3O_4 content in MEG-NH_2 nanohybrids on the adsorption of MEG-NH_2 nanohybrids for Ag(I) was studied at initial Ag(I) concentration of 40 mg·L^{-1}. As shown in Table 1, it can be clearly seen that the adsorption capacity of Ag(I) increased firstly and then decreased with the increasing of Fe_3O_4 content in MEG-NH_2 nanohybrids; it reached maximum when Fe_3O_4 content in MEG-NH_2 nanohybrids was 35.2%. Thus MEG-NH_2 nanohybrids with Fe_3O_4 content of 35.2% were used in the subsequent adsorption process.

3.3.2. Effect of pH. The pH value of aqueous solution is the premier parameter in adsorption studies and strongly affects the adsorption property of MEG-NH_2 nanohybrids. The effect of solution pH on the adsorption Ag(I) of MEG-NH_2 nanohybrids from aqueous solutions was investigated in the pH ranges of 1.0–7.0 at 25°C for 12 h as shown in

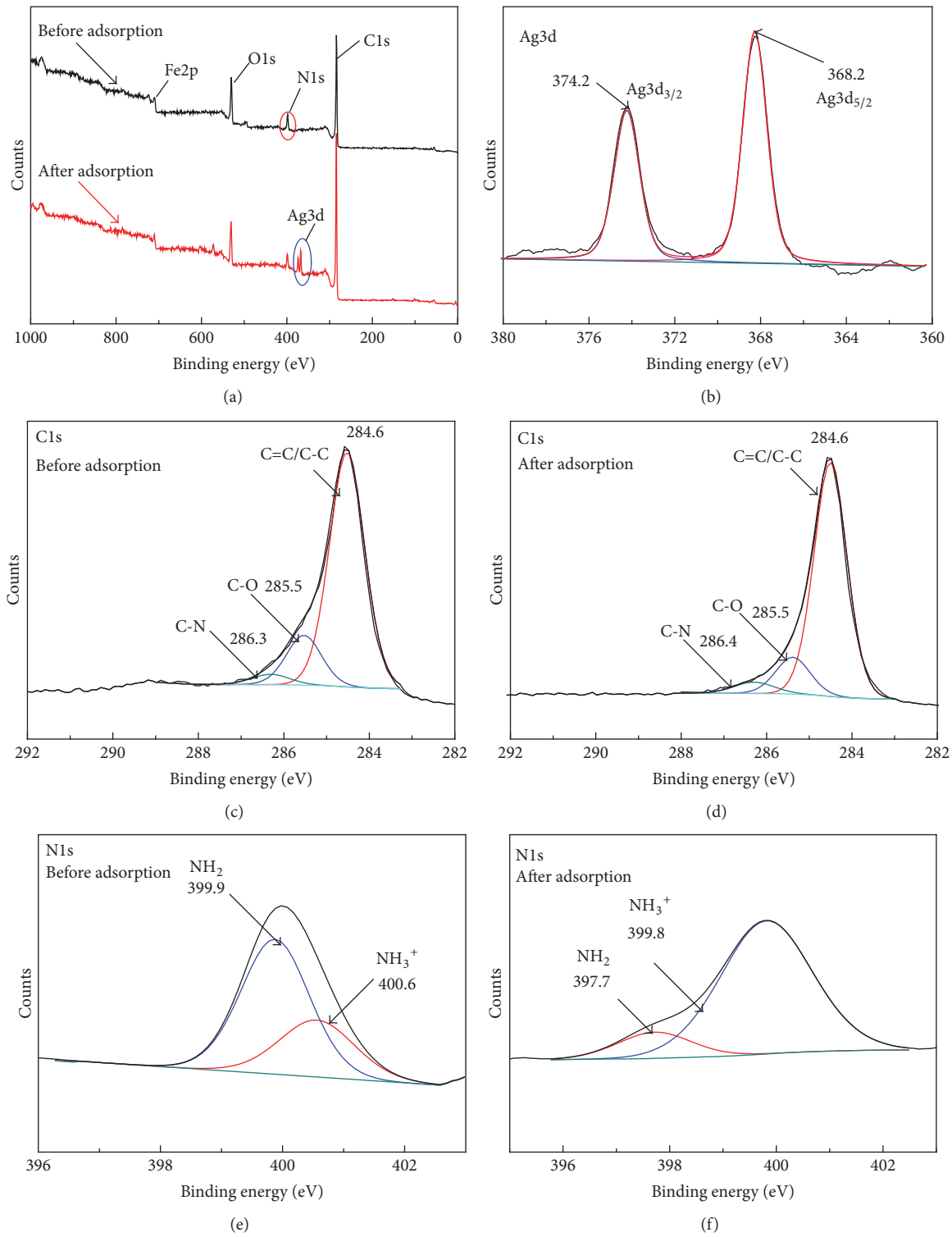

FIGURE 4: The survey XPS spectra of MEG-NH_2 nanohybrids and high-resolution XPS spectra of Ag3d (b), C1s (c, d), and N1s (e, f) before and after Ag(I) adsorption.

Figure 7. It can be seen clearly that the adsorption capacity increased with the pH increasing from 1.0 to 4.0 and reached a plateau value with pH range from 5.0 to 7.0. This phenomenon could be explained by the complex mechanism between Ag(I) and the donor atom (N) on surface of sample [30], which is relevant to interface protonation of the -NH_2 groups of MEG-NH_2 nanohybrids in the aqueous solution. From Figure 7 we can also see that the surface of MEG-NH_2 nanohybrids

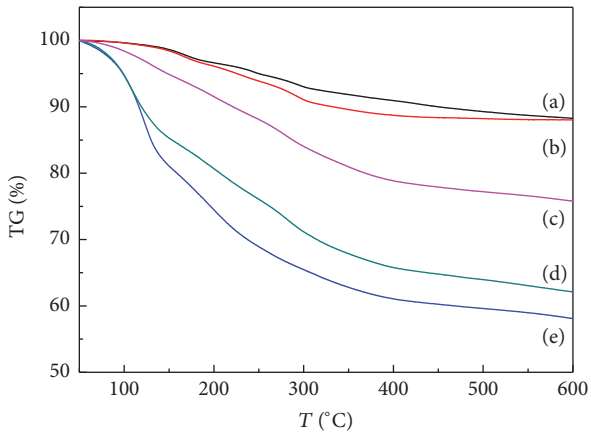

Figure 5: TGA curves of EG (a), Fe_3O_4-NH_2 (b), MEG-NH_2 nanohybrids prepared with 1.2 g (c), 1.0 g (d), and 0.8 g, and (e) $FeCl_3 \cdot 6H_2O$.

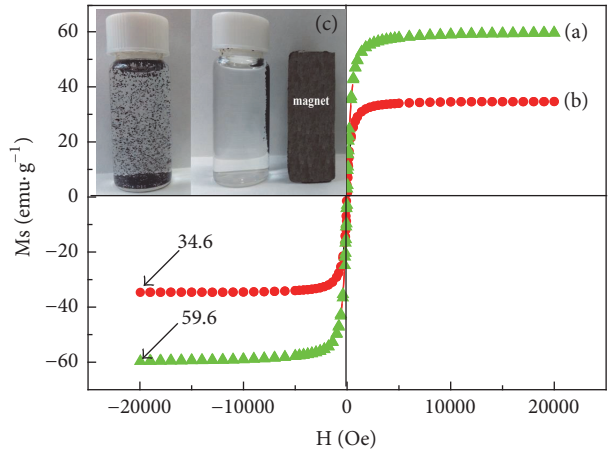

Figure 6: Magnetization curves of Fe_3O_4 nanoparticles (a) and MEG-NH_2 nanohybrids (b) at room temperature. The inset shows the photograph of MEG-NH_2 nanohybrids dispersion in the water (left) and their magnetic response placed in external magnetic field (right) (c).

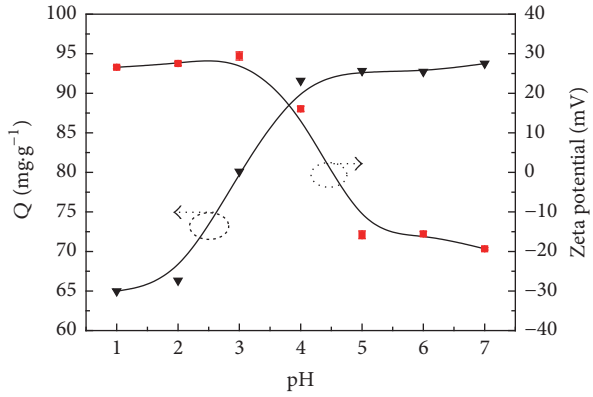

Figure 7: Effect of aqueous solution pH on the adsorption of MEG-NH_2 nanohybrids for Ag(I) and Zeta potentials of MEG-NH_2 nanohybrids.

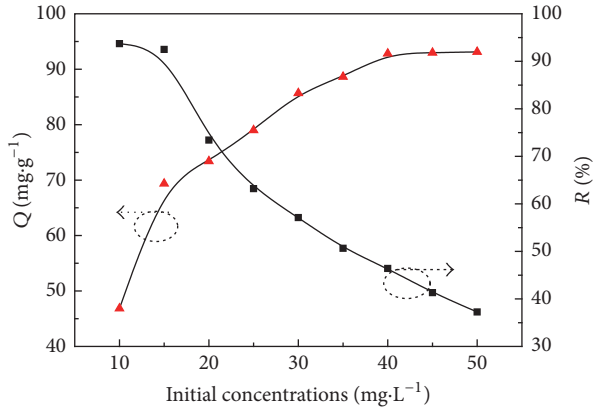

Figure 8: Effect of different initial concentration on the adsorption of MEG-NH_2 nanohybrids for Ag(I) (pH: 5.0, *m*: 10 mg, and temperature: 25°C).

is positively charged in the pH ranges of 1.0 to 4.0. At low pH, large number of H^+ protonated the -NH_2 groups on the surface of MEG-NH_2 nanohybrids; the transformation of -NH_2 into -NH_3^+ made the electrostatic attraction between MEG-NH_2 nanohybrids and Ag(I) was relatively weak and hindered the generation of metal complex. With the pH increasing, the number of positive charges on MEG-NH_2 nanohybrids decreased and the repulsion between Ag(I) and positive charge on MEG-NH_2 nanohybrids weakened, which contributed to -NH_2 groups on MEG-NH_2 nanohybrids coordination with Ag(I) and led to adsorption capacity increase. Further increasing the pH value from 5.0 to 7.0, the surface of MEG-NH_2 nanohybrids is negatively charged and the adsorption capacity reached a plateau value, which is possibly due to the fact that AgOH species formed have a higher formation constant and can steadily stay in the equilibrium solutions. Hence, pH 5.0 was determined as the optimal pH value in subsequent investigations.

3.3.3. Effect of Different Initial Concentrations. The effect of initial Ag(I) concentration (10, 20, 30, 40, and 50 mg·L^{-1}) in the solution on the adsorption of MEG-NH_2 nanohybrids is shown in Figure 8. With the increase of initial concentration, the adsorption capacity and removal rate presented opposite variation tendency. At the lowest Ag(I) concentration, the maximum removal rate was obtained, while the adsorption capacity was the minimum. The high removal rate was inclined to be acquired in the process of water treatment compared with adsorption capacity. So, the MEG-NH_2 nanohybrids are an ideal adsorbent to treat low Ag(I) concentration in aqueous solution.

3.3.4. Effect of Contact Time. The relationship between contact time and Ag(I) adsorption capacity of MEG-NH_2 nanohybrids at initial Ag(I) concentration of 40 mg·L^{-1} was presented in Figure 9. The adsorption capacity of MEG-NH_2 nanohybrids for Ag(I) ascended from 40.9 mg·g^{-1} to 90.0 mg·g^{-1} with increasing the contact time from 30 min to 360 min. Then, with time increasing, the adsorption capacity

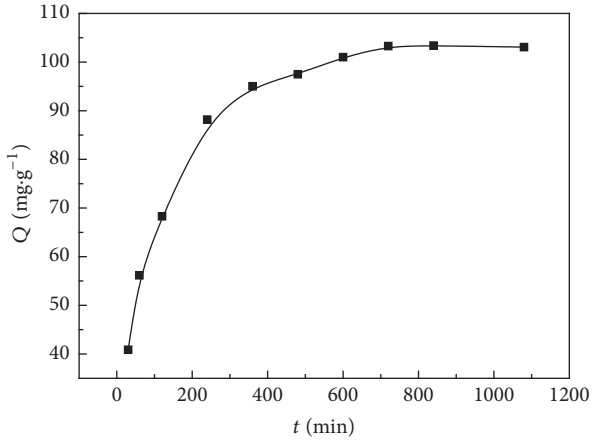

Figure 9: Effect of contact time on the adsorption of MEG-NH_2 nanohybrids for Ag(I) (C_0: 40 mg·L^{-1}, pH: 5.0, m: 10 mg, and temperature: 25°C).

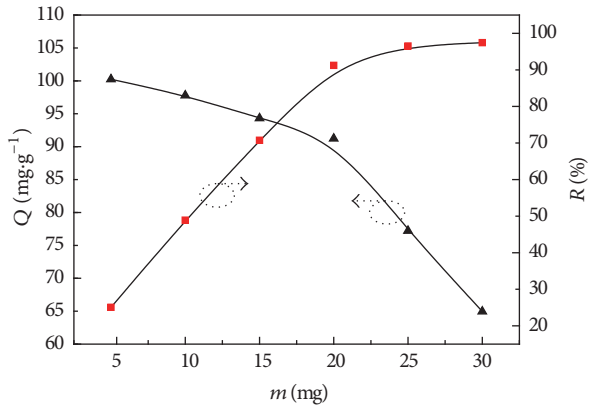

Figure 10: Effect of dosage on the adsorption of MEG-NH_2 nanohybrids for Ag(I) (C_0: 40 mg·L^{-1}, pH: 5, and temperature: 25°C).

of MEG-NH_2 nanohybrids for Ag(I) increased slowly till reaching equilibrium.

3.3.5. Effect of Dosage. In order to investigate the effect of dosage on the removal rate and adsorption capacity of MEG-NH_2 nanohybrids for Ag(I), different mass of MEG-NH_2 nanohybrids was added during the process of adsorption. The results are presented in Figure 10, from which, with the increase of the dosage of MEG-NH_2 nanohybrids, the removal rate and adsorption capacity presented opposite variation tendency. When the adsorbent mass was assigned to 5 mg, the adsorption capacity reached the maximum of 100.24 mg·g^{-1}, while the removal rate achieved the minimum value. Interestingly, when the dosage of adsorbent increased to 30 mg, the removal rate ascended gradually to the maximum of 97.4%, which was an ideal result. In contrast, the adsorption capacity descended to the minimum value. This meaningful phenomenon was generated because the quantity of Ag(I) in the aqueous solution was a constant, and, with the increase of adsorbent mass, the available active sites were also bound to increase to a considerable amount. Thus, the finite Ag(I) could be adsorbed efficiently and led to the removal rate increase and adsorption capacity decrease.

3.3.6. Adsorption Kinetics. In this study, in order to ascertain the most controlling mechanism for Ag(I) removal, pseudo-first-order and pseudo-second-order kinetics models were in application to fit the experimental data. Pseudo-first-order and pseudo-second-order kinetics were expressed as follows [6]:

$$Q_t = Q_e\left(1 - e^{-k_1 t}\right)$$
$$\frac{t}{Q_t} = \frac{1}{k_2 Q_e^2} + \frac{t}{Q_e}, \quad (2)$$

where k_1 (min^{-1}) and k_2 (g·mg^{-1}·min^{-1}) are the rate constant of adsorption of pseudo-first-order model and pseudo-second-order model, respectively. Q_e (mg·g^{-1}) is the equilibrium adsorption capacity and Q_t (mg·g^{-1}) is the adsorption capacity at time t.

The fitting curves are shown in Figure 11. The parameters and the correlation coefficients (R^2) of the two models are listed in Table 2. As shown in Figure 11 and Table 2; the adsorption of Ag(I) using MEG-NH_2 nanohybrids was well fitted by pseudo-second-order kinetics model with much higher correlation coefficient (0.999) than the pseudo-first-order kinetics (0.912) at the same conditions. The result indicates that the process controlling the rate was a chemical adsorption.

3.3.7. Adsorption Isotherms. To study the adsorption isotherms, the adsorption data in the concentration range from 10 to 50 mg·L^{-1} were fitted to Langmuir, Freundlich, Temkin, and Dubinin–Radushkevich isotherm models (Figure 12).

Langmuir isotherm was often applied to homogeneous adsorption surface with all the adsorptive sites qualified with equal affinity to adsorbate. The equation can be described as follows [31]:

$$\frac{C_e}{Q_e} = \frac{1}{Q_{\max} k_L} + \frac{C_e}{Q_{\max}}, \quad (3)$$

where Q_e (mg·g^{-1}) and C_e (mg·L^{-1}) are the equilibrium adsorption capacity and the equilibrium concentration of the adsorbate, while $Q_{\max}$ and K_L (mg·g^{-1}) represent the maximum adsorption capacity of adsorbent and the Langmuir adsorption constant (L·mg^{-1}), respectively. The values of $Q_{\max}$ and K_L are calculated from the slope and intercept of the linear plot of C_e/Q_e versus C_e.

Freundlich isotherm model assumes heterogeneity of adsorption surface, which is expressed as follows [32]:

$$Q_e = K_F C_e^{1/n}, \quad (4)$$

where Q_e (mg·g^{-1}) and C_e (mg·L^{-1}) are the amount of adsorbed Ag(I) and Ag(I) concentration at equilibrium, respectively. K_F and n are the Freundlich isotherm constants.

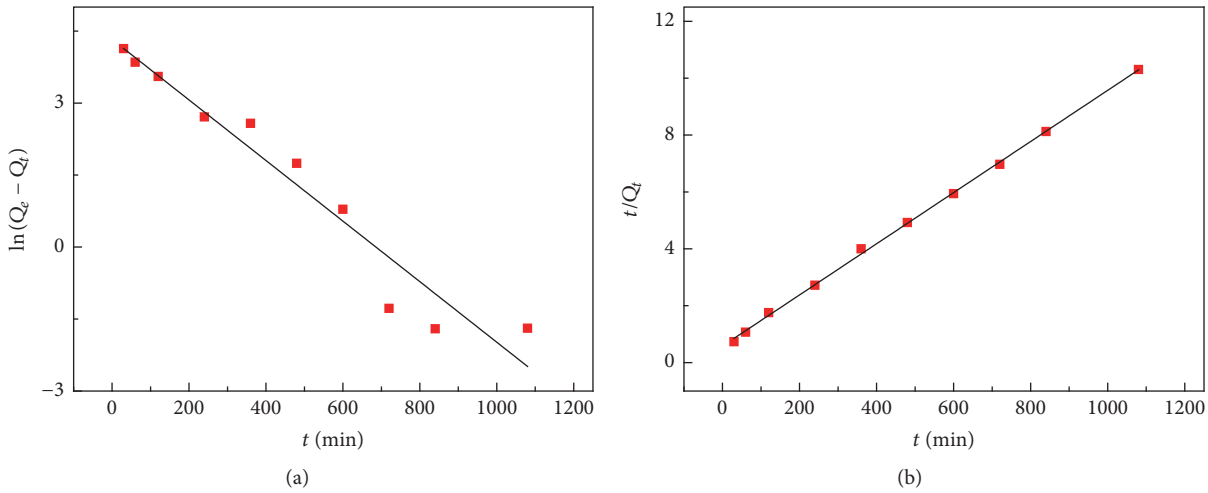

FIGURE 11: The kinetic models of pseudo-first-order (a) and pseudo-second-order (b) for adsorption of Ag(I) onto MEG-NH_2 nanohybrids.

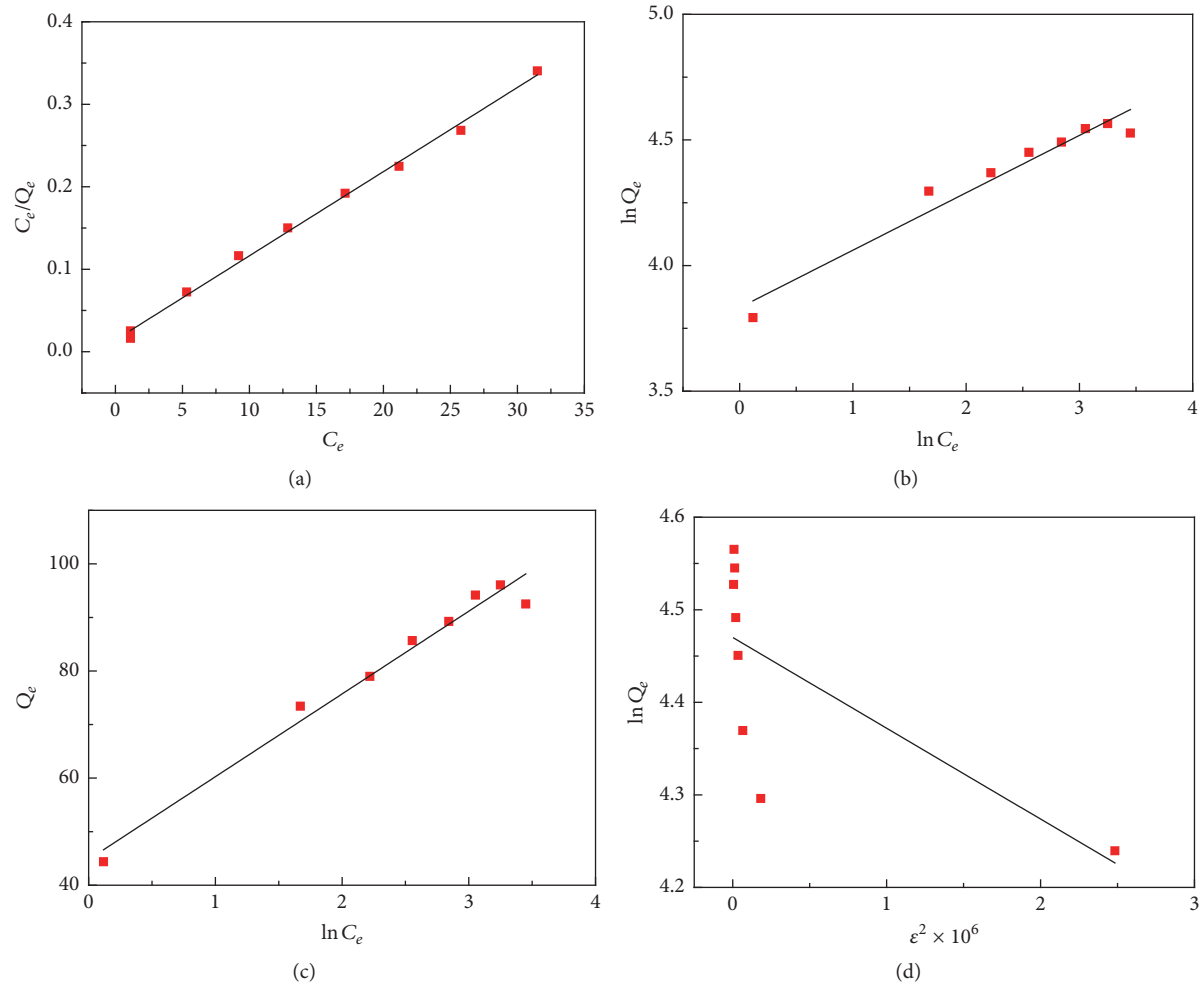

FIGURE 12: The isotherm models of Langmuir, Freundlich, Temkin, and Dubinin-Radushkevich for Ag(I) adsorption onto MEG-NH_2 nanohybrids.

Table 2: Pseudo-first-order and pseudo-second-order constants for Ag(I) adsorption at 25°C.

Pseudo-first-order			Pseudo-second-order			
R^2	k_1	Q_e (mg·g^{-1})	R^2	k_2	Q_e (mg·g^{-1})	Q_e (exp.) (mg·g^{-1})
0.912	0.021	99.073	0.999	2.904×10^{-4}	111.209	104.314

K_F value indicates the adsorption capacity and n is related to the energetic heterogeneity (average energy of sites). K_F and n can be achieved from the intercept and slope of the linear plot of ln Q against ln C.

The Temkin isotherm is determined by the following equation [33]:

$$Q = B \ln A_T + B \ln C, \tag{5}$$

where A_T is Temkin isotherm equilibrium binding constant (L·g^{-1}) and B is the constant related to heat of sorption (J·mol^{-1}).

Dubinin–Radushkevich isotherm is generally utilized to express the adsorption mechanism with a Gaussian energy distribution onto a heterogeneous surface. The model is represented by the following equation [34]:

$$\ln Q_e = \ln Q_s - K_{ad}\varepsilon^2$$
$$\varepsilon = RT \ln\left(1 + \frac{1}{C}\right), \tag{6}$$

where Q_e (mg·g^{-1}) and Q_s (mg·g^{-1}) are the amount of adsorbate in the adsorbent at equilibrium (mg·g^{-1}) and the theoretical isotherm saturation capacity (mg·g^{-1}), K_{ad} is the Dubinin–Radushkevich isotherm constant (mol^2·K^{-1}J^{-2}), ε is the Dubinin–Radushkevich isotherm constant, and R, T, and C represent the gas constant (8.314 J·mol^{-1}·K^{-1}), absolute temperature (K), and adsorbate equilibrium concentration (mg·L^{-1}), respectively.

Constants of all the isotherm models were listed in Table 3, which shows that the adsorption of Ag(I) on MEG-NH_2 nanohybrids fitted well to Langmuir isotherm model with a correlation coefficient R^2 value of 0.998. For comparison, the resulting correlation coefficients of the other three models at the same temperature of 25°C were lower than that of Langmuir isotherm model. The better fitting of Langmuir isotherm model reveals that the homogeneous adsorption surface with all the effective adsorption sites had identical adsorption energy and affinity. In addition, no interaction existed among adsorbate on the surface of MEG-NH_2 nanohybrids.

Table 3: Langmuir, Freundlich, Temkin, and Dubinin–Radushkevich isotherm parameters for Ag(I) adsorption onto MEG-NH_2 nanohybrids.

Isotherm	Parameters		R^2
Langmuir	Q_{max} (mg·g^{-1})	98.038	0.996
	K_L (L·g^{-1})	0.712	
Freundlich	K_f	46.181	0.942
	n	4.376	
Temkin	B_T (J·mol^{-1})	15.455	0.970
	A_T (L·g^{-1})	18.157	
Dubinin-Radushkevich	Q_{max} (mg·g^{-1})	99.058	0.852
	E (kJ·mol^{-1})	3.069	

4. Conclusions

(1) MEG-NH_2 nanohybrids were successfully fabricated by one-pot solvothermal method.

(2) Ag(I) was reduced to elemental silver in the process of the adsorption by MEG-NH_2 nanohybrids.

(3) The adsorption process could be better described by pseudo-second-order kinetics model and Langmuir isotherm model, which indicated that the adsorption process was a chemical adsorption on the homogeneous surface of MEG-NH_2 nanohybrids.

Competing Interests

The authors declare that there are no competing interests regarding the publication of this paper.

Acknowledgments

This work was supported by the National Natural Science Foundation of China (51403091) and the Postdoctoral Science Foundation of China (2015M572616).

References

[1] M. Yurtsever and A. I. Şengil, "Adsorption and desorption behavior of silver ions onto valonia tannin resin," *Transactions of Nonferrous Metals Society of China*, vol. 22, no. 11, pp. 2846–2854, 2012.

[2] M. H. Beyki, M. Bayat, S. Miri, F. Shemirani, and H. Alijani, "Synthesis, characterization, and silver adsorption property of magnetic cellulose xanthate from acidic solution: prepared by one step and biogenic approach," *Industrial & Engineering Chemistry Research*, vol. 53, no. 39, pp. 14904–14912, 2014.

[3] H.-C. Tao, Z.-Y. Gao, H. Ding, N. Xu, and W.-M. Wu, "Recovery of silver from silver(I)-containing solutions in bioelectrochemical reactors," *Bioresource Technology*, vol. 111, no. 3, pp. 92–97, 2012.

[4] O. N. Kononova, K. A. Shatnykh, K. V. Prikhod'Ko, and D. M. Kashirin, "Ion-exchange recovery of gold(I) and silver(I) from thiosulfate solutions," *Russian Journal of Physical Chemistry A*, vol. 83, no. 13, pp. 2340–2345, 2009.

[5] H.-I. Song, B.-J. Min, S.-Y. Cho, and P.-P. Sun, "Solvent extraction of silver from nitric acid solution with 5,8-diethyl-7-hydroxy-dodecan-6-oxime," *Journal of Chemical Engineering of Japan*, vol. 48, no. 10, pp. 829–833, 2015.

[6] C. Zhang, J. Sui, J. Li, Y. Tang, and W. Cai, "Efficient removal of heavy metal ions by thiol-functionalized superparamagnetic carbon nanotubes," *Chemical Engineering Journal*, vol. 210, no. 4, pp. 45–52, 2012.

[7] A. M. Donia, A. A. Atia, and K. Z. Elwakeel, "Recovery of gold(III) and silver(I) on a chemically modified chitosan with magnetic properties," *Hydrometallurgy*, vol. 87, no. 3-4, pp. 197–206, 2007.

[8] H. B. Hou, D. M. Yu, and G. H. Hu, "Preparation and properties of ion-imprinted hollow particles for the selective adsorption of silver ions," *Langmuir*, vol. 31, no. 4, pp. 1376–1384, 2015.

[9] M. A. Abd El-Ghaffar, Z. H. Abdel-Wahab, and K. Z. Elwakeel, "Extraction and separation studies of silver(I) and copper(II) from their aqueous solution using chemically modified melamine resins," *Hydrometallurgy*, vol. 96, no. 1-2, pp. 27–34, 2009.

[10] T. Kanjilal, S. Babu, K. Biswas, C. Bhattacharjee, and S. Datta, "Application of mango seed integuments as bio-adsorbent in lead removal from industrial effluent," *Desalination and Water Treatment*, vol. 56, no. 4, pp. 984–996, 2015.

[11] G. Qi, W. Zhang, and Y. Dai, "Synthesis of magnetic expanded graphite and its application to remove Cr(VI) from wastewater," *Synthesis and Reactivity in Inorganic, Metal-Organic and Nano-Metal Chemistry*, vol. 44, no. 1, pp. 153–160, 2014.

[12] X.-B. Wang, W.-F. Zhu, X. Wei, Y.-X. Zhang, and H.-H. Chen, "Preparation and millimeter wave attenuation properties of $NiFe_2O_4$/expanded graphite composites by low-temperature combustion synthesis," *Materials Science and Engineering: B*, vol. 185, no. 1, pp. 1–6, 2014.

[13] V. K. Singh and P. N. Tiwari, "Removal and recovery of chromium(VI) from industrial waste water," *Journal of Chemical Technology & Biotechnology*, vol. 69, no. 3, pp. 376–382, 1997.

[14] J. L. Chang, J. C. Ma, Q. L. Ma et al., "Adsorption of methylene blue onto Fe_3O_4/activated montmorillonite nanocomposite," *Applied Clay Science*, vol. 119, pp. 132–140, 2016.

[15] Y.-X. Ma, Y.-F. Li, G.-H. Zhao et al., "Preparation and characterization of graphite nanosheets decorated with Fe_3O_4 nanoparticles used in the immobilization of glucoamylase," *Carbon*, vol. 50, no. 8, pp. 2976–2986, 2012.

[16] S. Pan, Y. Zhang, H. Shen, and M. Hu, "An intensive study on the magnetic effect of mercapto-functionalized nano-magnetic Fe_3O_4 polymers and their adsorption mechanism for the removal of Hg(II) from aqueous solution," *Chemical Engineering Journal*, vol. 210, no. 6, pp. 564–574, 2012.

[17] X. Li, Z. Wang, Q. Li, J. Ma, and M. Zhu, "Preparation, characterization, and application of mesoporous silica-grafted graphene oxide for highly selective lead adsorption," *Chemical Engineering Journal*, vol. 273, pp. 630–637, 2015.

[18] L. Wang, X. Fu, E. Chang et al., "Preparation and its adsorptive property of modified expanded graphite nanomaterials," *Journal of Chemistry*, vol. 2014, Article ID 678151, 5 pages, 2014.

[19] I. M. Afanasov, O. N. Shornikova, V. V. Avdeev, O. I. Lebedev, G. Van Tendeloo, and A. T. Matveev, "Expanded graphite as a support for Ni/carbon composites," *Carbon*, vol. 47, no. 2, pp. 513–518, 2009.

[20] X. Guo, B. Du, Q. Wei et al., "Synthesis of amino functionalized magnetic graphenes composite material and its application to remove Cr(VI), Pb(II), Hg(II), Cd(II) and Ni(II) from contaminated water," *Journal of Hazardous Materials*, vol. 278, pp. 211–220, 2014.

[21] I. F. Nata, G. W. Salim, and C.-K. Lee, "Facile preparation of magnetic carbonaceous nanoparticles for Pb^{2+} ions removal," *Journal of Hazardous Materials*, vol. 183, no. 1–3, pp. 853–858, 2010.

[22] R. J. Wang, Y. X. Ma, C. P. Lu, T. Li, and X. Y. Du, "Preparation and adsorption property of glutathione magnetic molecularly imprinted polymers," *Acta Chimica Sinica*, vol. 72, no. 5, pp. 577–582, 2014.

[23] S. Makharza, G. Cirillo, A. Bachmatiuk et al., "Graphene oxide-based drug delivery vehicles: functionalization, characterization, and cytotoxicity evaluation," *Journal of Nanoparticle Research*, vol. 15, no. 12, pp. 13982–13989, 2013.

[24] L. Zeng, Y. Chen, Q. Zhang et al., "Adsorption of Cd(II), Cu(II) and Ni(II) ions by cross-linking chitosan/rectorite nano-hybrid composite microspheres," *Carbohydrate Polymers*, vol. 130, pp. 333–343, 2015.

[25] X. L. Li, *Preparation of novel composite adsorbents based on polymer matrix and the research on the adsorption of heavy metals in aqueous solutions [Ph.D. thesis]*, Lanzhou University, 2013.

[26] Y. Wang, X. Ma, Y. Li et al., "Preparation of a novel chelating resin containing amidoxime-guanidine group and its recovery properties for silver ions in aqueous solution," *Chemical Engineering Journal*, vol. 209, pp. 394–400, 2012.

[27] T. Fujii, F. M. F. De Groot, G. A. Sawatzky, F. C. Voogt, T. Hibma, and K. Okada, "In situ XPS analysis of various iron oxide films grown by NO_2-assisted molecular-beam epitaxy," *Physical Review B*, vol. 59, no. 4, pp. 3195–3202, 1999.

[28] K. Gul, S. Sohni, M. Waqar, F. Ahmad, N. A. N. Norulaini, and A. K. M. Omar, "Functionalization of magnetic chitosan with graphene oxide for removal of cationic and anionic dyes from aqueous solution," *Carbohydrate Polymers*, vol. 152, pp. 520–531, 2016.

[29] H. Bagheri, A. Afkhami, P. Hashemi, and M. Ghanei, "Simultaneous and sensitive determination of melatonin and dopamine with Fe_3O_4 nanoparticle-decorated reduced graphene oxide modified electrode," *RSC Advances*, vol. 5, no. 28, pp. 21659–21669, 2015.

[30] A. M. Donia, A. M. Yousif, A. A. Atia, and M. F. Elsamalehy, "Efficient adsorption of Ag(I) and Au(III) on modified magnetic chitosan with amine functionalities," *Desalination & Water Treatment*, vol. 52, no. 13–15, pp. 2537–2547, 2014.

[31] S. Luo, X. Xu, G. Zhou, C. Liu, Y. Tang, and Y. Liu, "Amino siloxane oligomer-linked graphene oxide as an efficient adsorbent for removal of Pb(II) from wastewater," *Journal of Hazardous Materials*, vol. 274, no. 12, pp. 145–155, 2014.

[32] M. Firlak, M. V. Kahraman, E. K. Yetimoğlu, and B. Zeytuncu, "Adsorption of Ag (I) ions from aqueous solutions using photocured thiol-ene hydrogel," *Separation Science & Technology*, vol. 48, no. 18, pp. 2860–2870, 2013.

[33] A. Günay, E. Arslankaya, and I. Tosun, "Lead removal from aqueous solution by natural and pretreated clinoptilolite: adsorption equilibrium and kinetics," *Journal of Hazardous Materials*, vol. 146, no. 1-2, pp. 362–371, 2007.

[34] A. O. Dada, A. P. Olalekan, A. M. Olatunya, and O. Dada, "Langmuir, Freundlich, Temkin and Dubinin-Radushkevich isotherms studies of equilibrium sorption of Zn^{2+} onto phosphoric acid modified rice husk," *Journal of Applied Chemistry*, vol. 3, pp. 38–45, 2012.